

# Chromium-Coated Cladding Analysis under Simulated LOCA Burst Conditions

Ryan Sweet<sup>1</sup>, Peter Mouche<sup>1</sup>, Samuel Bell<sup>2</sup>, Kenneth Kane<sup>1</sup> and Nathan Capps<sup>1,2</sup>

<sup>1</sup>Oak Ridge National Laboratory

<sup>2</sup>University of Tennessee, Knoxville

## Abstract

Of the near-term accident-tolerant fuel concepts identified, chromium coatings have been shown to slow cladding oxidation without altering fuel system geometry or greatly affecting neutronic performance. To identify how coated cladding tubes perform under high-temperature accident conditions, pressurized-tube burst tests were conducted in the Severe Accident Test Station at Oak Ridge National Laboratory. To analyze how the coating affects cladding behavior, coated and uncoated cladding burst tests were simulated by using the BISON fuel performance code. Thermocouple data from these tests were fit into axial and azimuthal profiles and combined to generate 3D cladding surface temperatures, and pressure transducer data were compared until cladding failure. The cladding temperatures at failure and the internal gas pressure evolution show relatively good agreement between the simulation and experiment results. Simulations were then extrapolated to demonstrate the coatings effectiveness to increasing the cladding burst temperature by using a parametric evaluation of the initial tube gas pressure. This work demonstrates the possibility of an increased cladding failure margin under transient conditions due to the addition of chromium coating, and more pertinently, an increased cladding failure margin from more accurate experimental characterization.

## 1. INTRODUCTION

As a result of the events at the Fukushima Daiichi Nuclear Power Plant in 2011, an international effort was initiated to develop accident-tolerant fuel (ATF) concepts to minimize and possibly mitigate accident consequences by significantly reducing the high-temperature steam oxidation of zirconium-based cladding and structural materials. The oxidation reaction of zirconium-based alloys (Zircaloy) components is exothermic and releases hydrogen gas when zirconium and oxygen react. As zirconium heats above 1,200°C, the oxidation reaction kinetics reach a rate at which the heat released from the reaction further increases the cladding temperature, creating a thermal feedback cycle and becoming autocatalytic. The reaction continues to release energy and generate hydrogen as the zirconium is consumed [1, 2]. Finally, the generated hydrogen gas may eventually ignite as it increases in concentration [3]. Multiple strategies have been proposed to improve the cladding response under beyond design basis accidents (BDBAs), such as using alternative materials for fuel cladding or coating the outside of the current zirconium-based alloys [4]. Along with the improved performance during BDBAs, these strategies may further enhance safety and economic benefits during design basis accidents and normal operation, allowing nuclear power plants to operate more efficiently and improve the economic viability of nuclear power.

Chromium-coated Zircaloy cladding tubes are a leading ATF candidate because chromium offers superior oxidation kinetics and is compatible with the Zircaloy cladding substrate [5]. Chromium forms a very thin (<1 μm) passivating oxide layer, Cr<sub>2</sub>O<sub>3</sub>, which allows the coating thickness to be relatively thin for the

This manuscript has been authored by UT-Battelle, LLC under Contract No. DE-AC05-00OR22725 with the US Department of Energy (DOE). The US government retains and the publisher, by accepting the article for publication, acknowledges that the US government retains a nonexclusive, paid-up, irrevocable, worldwide license to publish or reproduce the published form of this manuscript, or allow others to do so, for US Government purposes. DOE will provide public access to these results of federally sponsored research in accordance with the DOE Public Access Plan (<http://energy.gov/downloads/doe-public-access-plan>).

<sup>2</sup> Corresponding author: [cappsna@ornl.gov](mailto:cappsna@ornl.gov)

cladding tube to see significant benefits. Thin coatings minimize the neutronic penalty from the thermal neutron absorption of chromium and allow chromium-coated Zircaloy to be a drop-in replacement for current fuel rod designs without geometric reconfiguration. However, several coating performance issues must be addressed before full-core deployment, such as cladding coating chemical interactions, irradiation behavior, and coating performance during transient scenarios [6].

If the coating remains adherent during normal operation and DBAs, the oxidation behavior of chromium-coated cladding is expected to be significantly reduced compared with existing fuel rod materials. Because the coating is relatively thin, it should not have any thermal or mechanical impact during normal operation if there is no significant chemical interaction with the cladding substrate. The fuel rod transient behavior is different, and high stresses and strains on the coating may be induced, resulting in cracking, delamination, or spallation of the coating. Particularly, a loss-of-coolant accident (LOCA) may result in excessive local strains that form in the cladding due to high internal gas pressure, leading to rupture as cladding temperatures increase. As the accident progresses and cladding temperatures rise, the cladding begins to form a ballooned region in which the cladding will subsequently rupture, releasing the internal pressure. [3]. During this deformation process, it is hypothesized that the coating will fracture extensively and potentially delaminate from the substrate. This would allow water and steam to react with the unoxidized Zircaloy substrate, which will rapidly oxidize [5]. However, because the coating increases cladding structural stability at high temperatures, the cladding deformation rate and balloon size at failure may be reduced, prolonging cladding rupture. By reducing the cladding ballooning and increasing the rupture temperatures, chromium coatings might offer support toward the industries' high-burnup safety case and could reduce the effect of high-burnup fuel fragmentation relocation and dispersal consequences.

This paper discusses the enhanced burst behavior afforded by chromium-coated Zircaloy-4 (Zry-4) by coupling experimental data to modeling and simulation efforts. Then, it compares Zry-4 and chromium-coated Zry-4 under simulated burst test conditions. LOCA burst tests were performed on several bare Zry-4 and chromium-coated Zry-4 cladding tubes. These tests were subsequently simulated via the BISON fuel performance code and compared with the experimental data. The purpose of this comparison is twofold: (1) it validates BISON's ability to appropriately model coated cladding tubes that use multilayered materials while assessing material model predictions, and (2) it helps identify potential increases of the cladding margin to burst from the addition of the coating. These simulations are performed by developing more accurate conditions and better defining rupture temperature and strain conditions to assess the cladding failure margin more accurately.

## **2. MODELING APPROACH**

### **2.1 SEVERE ACCIDENT TEST STATION DATA**

To assess the cladding response during the burst tests using BISON, a model and boundary conditions were first constructed from LOCA experiments. Data generated from simulated LOCA experiments performed in the Severe Accident Test Station (SATS) at Oak Ridge National Laboratory (ORNL) were used to develop these conditions [7]. SATS LOCA experiments heat a pressurized cladding tube specimen with a multielement infrared furnace until the cladding ruptures. Experiments continue beyond cladding rupture to assess post-rupture oxidation and post-quench ductility. Cladding tube samples can be 3–12 in. (~7–30 cm) long and enclose an alumina rod with an 8 mm outer diameter that spans the length of the tube. The burst tests discussed in this paper used cladding tube sample lengths of 12 in. (~30 cm) and were heated to a terminal temperature of 1,200°C. A diagram of the SATS LOCA furnace setup is shown in Figure 1 [8]. Tests performed in the SATS use a pressure transducer located outside the furnace to measure in situ rod internal pressure.

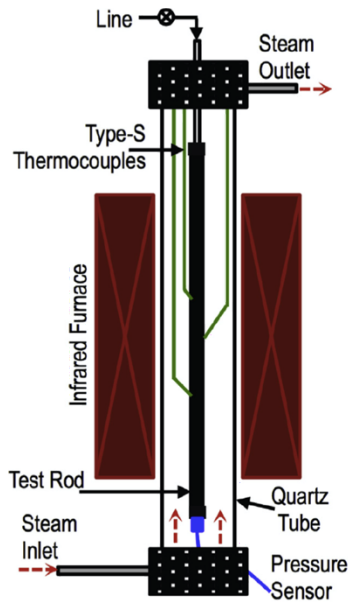


**Figure 1. Diagram of the Severe Accident Test Station setup.**  
 (Reproduced from: C. P. Massey et al., *Journal of Nuclear Materials*  
 470 (2016): 128–138)

Each cladding tube is instrumented with four thermocouples: three along the axial length and one placed 180° azimuthally across the tube midplane. The side of the cladding tube instrumented with the three thermocouples is placed facing the back of the furnace, and the single thermocouple faces the furnace entrance at front of the furnace. The thermocouples placed in the back of the furnace along the axial length of the tube are intended to measure the cladding temperature across the central 4 in. (~10.2 cm) of the tube length. The middle thermocouple is located at the cladding midplane, approximately 6 in. (~15.2 cm) from the bottom of the cladding tube, and the top and bottom thermocouples are 2 in. (~5.1 cm) above and below the middle thermocouple. Figure 2 provides a schematic of the thermocouple locations. The most common burst location is typically located on the back side of the tube between the center and bottom thermocouple locations. This is important because the cladding is expected to experience the greatest deformation and failure in the hottest region.

This manuscript has been authored by UT-Battelle, LLC under Contract No. DE-AC05-00OR22725 with the US Department of Energy (DOE). The US government retains and the publisher, by accepting the article for publication, acknowledges that the US government retains a nonexclusive, paid-up, irrevocable, worldwide license to publish or reproduce the published form of this manuscript, or allow others to do so, for US Government purposes. DOE will provide public access to these results of federally sponsored research in accordance with the DOE Public Access Plan (<http://energy.gov/downloads/doe-public-access-plan>).

<sup>2</sup> Corresponding author: [cappsna@ornl.gov](mailto:cappsna@ornl.gov)

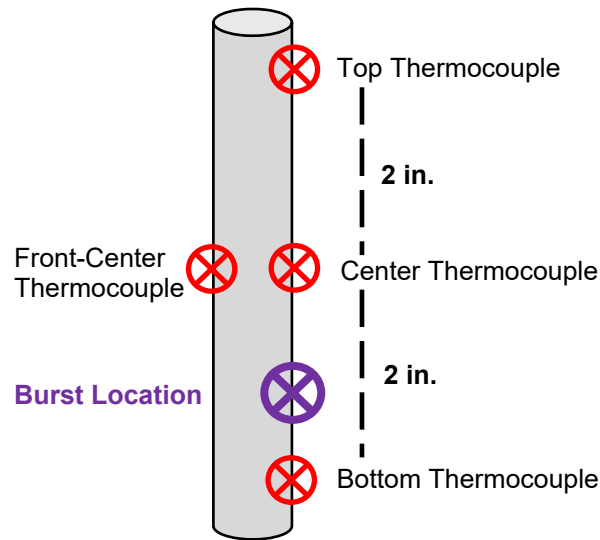


**Figure 2. Schematic of the thermocouple placement and burst location on the center 4 in. (~10.2 cm) section of the 12 in. (~30.5 cm) cladding test specimen used in the Severe Accident Test Station.**

Test initiation begins with pressurizing and heating the cladding tubes. The cladding is heated to 573 K and held for ~5 min to give the test administrators time to check for pressure leaks and ensure that the rod internal pressure is consistent with the test matrix. Eventually, the cladding tube is sealed and heated at a specified rate, typically 5°C/s, according to the control thermocouple (in this case, the middle rear thermocouple), and flowing steam heated to 673 K is injected into the quartz tube chamber. The cladding is heated to ~1,200°C (1,473 K) and held constant for ~5 min, and then the furnace is deactivated, allowing the cladding to air cool. Once the cladding control thermocouple reaches 873 K, the flowing steam is shut off, and the tube is quenched in room-temperature distilled water. SATS tests using this same approach were run on a variety of coated and uncoated cladding tubes with various alloy substrates and different initial pressures. Other parameters (e.g., heating rates, hold times, quench time, terminal temperature) could be controlled to fulfil the test objects; however, the aforementioned description is applicable to standard LOCA test procedures.

During the initial heat-up phase, the cladding tube begins to thermally expand as the temperature increases. A small amount of elastic expansion occurs due to the internal gas pressure on the cladding. The measured gas expansion does not directly track with the absolute temperature because the majority of the gas in the system remains in fixtures and gas lines outside the furnace itself. Figure 3 provides an example of the data acquired over time from a standard LOCA test in the SATS. In the figure, the left axis indicates the recorded temperatures for the four thermocouples over the first 700 s for an uncoated Zr-4 tube with an initial pressure of 800 psi (~5.5 MPa), and the right axis shows the data recorded by the pressure transducer. The increasing gas pressure coupled with the increasing cladding temperature results in an increasing thermal creep rate, allowing the cladding to radially expand and eventually balloon and burst. Rupture can be identified in Figure 3 by the transient thermocouple measurements and rapid depressurization measured by the pressure transducer. The temperature transient is driven by rapid expansion of the cladding during the rupture event followed by the release of gas stored in the system, which is cooler than the cladding. The high-temperature and cool-down data are not very relevant to the cladding bursting behavior, so these data are not included in this paper.

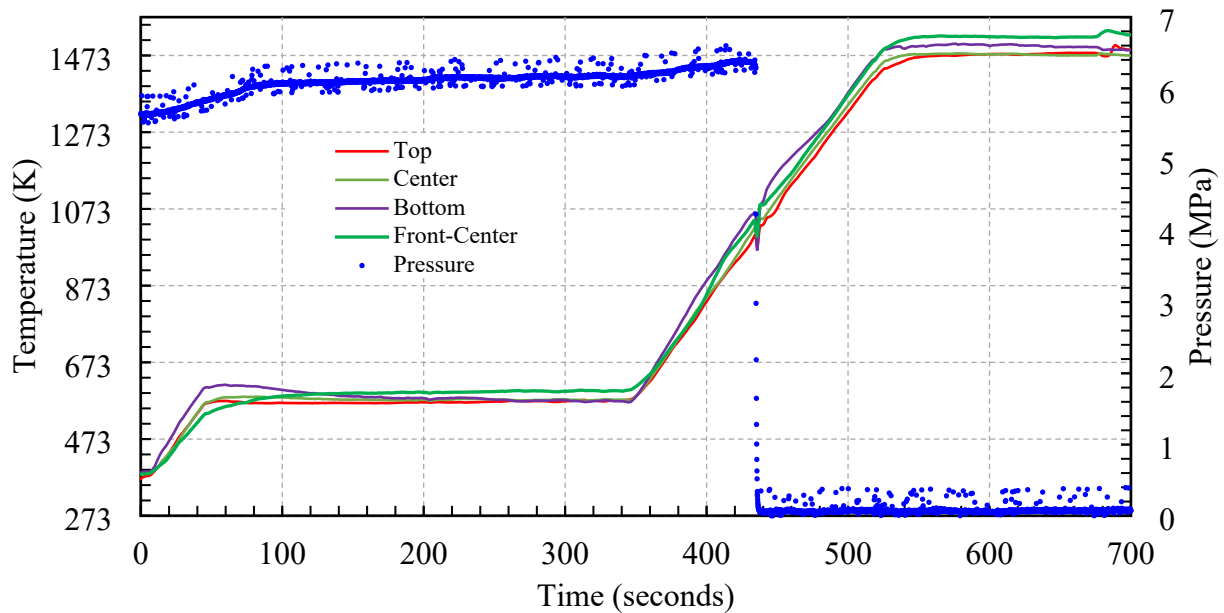


**Figure 3. Example of thermocouple and pressure data generated from the uncoated 800 psi Zr-4 burst test.**

Tube characteristics for chromium-coated and uncoated cladding tubes from previous tests in the SATS are shown in Table 1. The substrate cladding tube was 575  $\mu\text{m}$  thick, and chromium-coated Zircaloy tubes had an additional 7  $\mu\text{m}$  chromium coating applied to the exterior surface, making the total thickness 582  $\mu\text{m}$ . The initial rod internal pressures ranged from 600 to 1,600 psi (4.1 to 11 MPa).

**Table 1. Cladding properties and geometry used in the SATS.**

Cladding properties	Value
Substrate material	Zry-4
Inner radius (mm)	4.175
Outer radius (mm)	4.750
Cladding thickness (mm)	0.575
Cladding length (cm)	30.48
Coating thickness ( $\mu\text{m}$ )	7
<i>(if applied)</i>	

This manuscript has been authored by UT-Battelle, LLC under Contract No. DE-AC05-00OR22725 with the US Department of Energy (DOE). The US government retains and the publisher, by accepting the article for publication, acknowledges that the US government retains a nonexclusive, paid-up, irrevocable, worldwide license to publish or reproduce the published form of this manuscript, or allow others to do so, for US Government purposes. DOE will provide public access to these results of federally sponsored research in accordance with the DOE Public Access Plan (<http://energy.gov/downloads/doe-public-access-plan>).

<sup>2</sup> Corresponding author: [cappsna@ornl.gov](mailto:cappsna@ornl.gov)

Coatings were deposited onto the outside of 12” long tubes by Acrec Technologies Inc using high-power impulse magnetron sputtering (HiPIMS) to a thickness of 7  $\mu\text{m}$ . A two-axis planetary stage with central shield was used to evenly coat all sides of the tubes while limiting the path length of the Cr ions from the target to the samples to maintain ion energy. This helped to maximize coating density and residual stress imparted by energetic ions typical of the HiPIMS deposition method.

Four reference samples were cut from the length of one of the tubes with a low-speed diamond saw, mounted in epoxy, and polished. SEM images were taken around the circumference of each sample, see Figure 4. Coating thickness was observed to be very uniform along the circumference and length of the tubes. The high aspect ratio grooves observed from the surface analysis was found to introduce breaks in the coating due to the line-of-site nature of sputtering techniques. However, it was decided that these coatings would serve as a worst cases scenario during a simulated LOCA test, and therefore, it was decided to proceed with these samples to ensure the underlying substrate was not impacted by the defected coating.

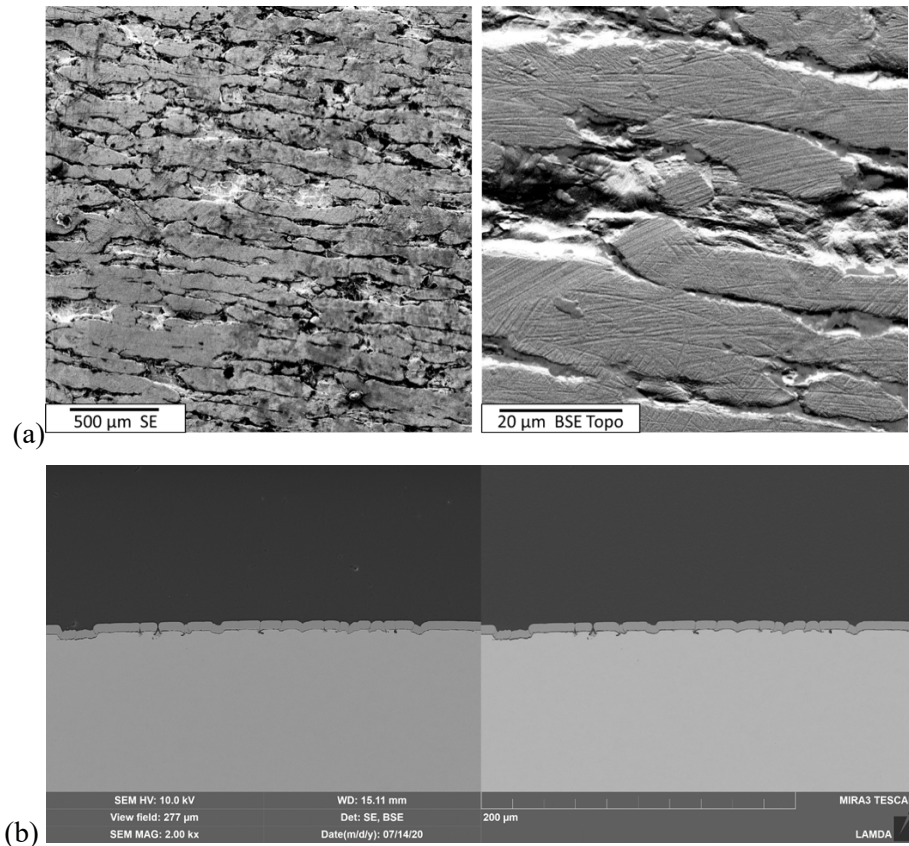


**Figure 4. a) Secondary (SE), top right, and backscatter topological (BSE Topo), top left, images of the tube surfaces showing high aspect ratio grooves on as received Zircaloy samples, and b) circumferential SEM image of showing extensive delamination at the bonding interface.**

## 2.2 SURFACE TEMPERATURE PROFILE DEVELOPMENT

As mentioned previously, the three thermocouples on the back of the cladding are centered at the cladding midplane and provide local temperatures for a 4 in. (~10 cm) span of the tube. Figure 5 shows X's marking the location of the thermocouples as well as the impact of the thermocouples on the balloon behavior. Because there are no temperature data for the end segments of the tube, thermocouple data from each SATS experiment were used to develop a continuous temperature shape. Additionally, the midplane thermocouples were used to develop an azimuthal temperature variation. The resulting axial and

azimuthal temperature shapes were used together to generate a fully 3D cladding surface temperature to accurately replicate the LOCA burst test. Traditionally, linear interpolation is used to define the temperature between thermocouples; however, the cladding burst does not occur at the thermocouple locations and instead typically occurs between thermocouples. This is likely a result of the actual peak temperature at the rupture location, which is not measured. The burst locations in these tests show a degree of reproducibility, indicating that that failure is not due to preexisting flaws or preparation. Therefore, the proposed method intends to develop an improved pressure and burst comparison by creating a complete cladding surface temperature to accurately calculate internal pressure and stain evolution during the LOCA test.



**Figure 5. Post LOCA image of a Cr-coated Zircaloy 4 tube sampled with X's marking the location of thermocouples**

The axial temperature profiles were generated by using a fourth-order polynomial, and the thermocouple measurements were imposed as constraints. In parallel, preliminary measurements using a fiber-optic temperature sensor suggested that the ends of the cladding tube fall within 60–80% of the nearest thermocouple temperature. Although this is a significant approximation, the ends of the cladding tube are located outside the infrared (IR) furnace and are expected to be significantly cooler than the middle sections. Therefore, the ends of the cladding will not experience significant thermal creep deformation, and the cladding end temperatures will only affect the gas expansion calculations. Figure 6 shows a selected axial temperature profile to demonstrate the shape along with the thermocouples. This profile was selected because it demonstrates a very defined temperature gradient in which the peak temperature is greater than the peak thermocouple temperature and present at a different location. Figure 6 illustrates the three thermocouple temperatures as red circles and the fitted cladding temperature profile as a blue line. Additionally, the peak temperature location is found between the bottom and middle thermocouple, which is consistent with the reported burst location.

This manuscript has been authored by UT-Battelle, LLC under Contract No. DE-AC05-00OR22725 with the US Department of Energy (DOE). The US government retains and the publisher, by accepting the article for publication, acknowledges that the US government retains a nonexclusive, paid-up, irrevocable, worldwide license to publish or reproduce the published form of this manuscript, or allow others to do so, for US Government purposes. DOE will provide public access to these results of federally sponsored research in accordance with the DOE Public Access Plan (<http://energy.gov/downloads/doe-public-access-plan>).

<sup>2</sup> Corresponding author: [cappsna@ornl.gov](mailto:cappsna@ornl.gov)

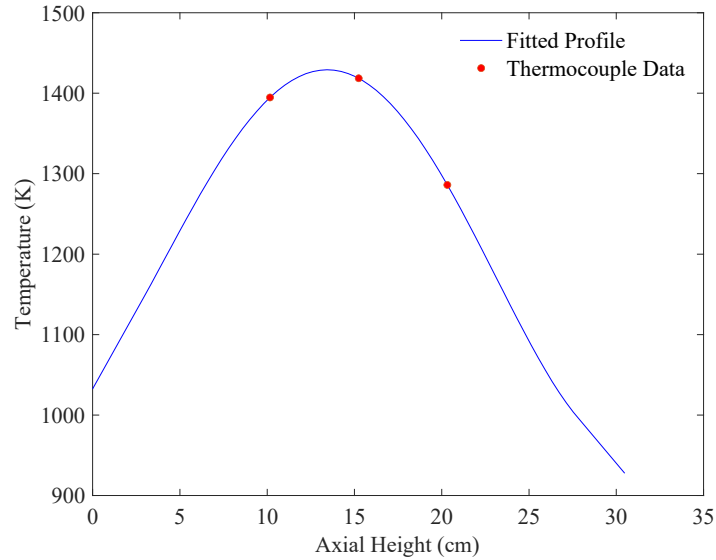


**Figure 6. Example of the fitted axial profile compared with the thermocouple data generated in the Severe Accident Test Station where the axial height is in relation to the bottom (0 cm) to the top (~30 cm) of the rod.**

Figure 3 indicates the thermocouple measurements quite frequently in time and in relation to each other, and as a result, the axial profiles do not remain constant and change at every time step. Each experiment extracts thermocouple and pressure transducer data sampled at 0.1 s intervals. The axial fitting method is applied to these data, resulting in axially varying cladding temperatures as a function of time for the SATS LOCA test. Figure 7 illustrates the maximum and minimum axial temperatures for a sample rod at each time step over the experiment time frame considered in this analysis. A temperature jump is observed when the cladding sample ruptures as the fill gas is released through the rupture opening. The thermocouple temperature variation over this short time is interpolated linearly to remove the effect of the gas release. This ensures that the calculations are not influenced by the temperature variations caused by the sudden gas release.

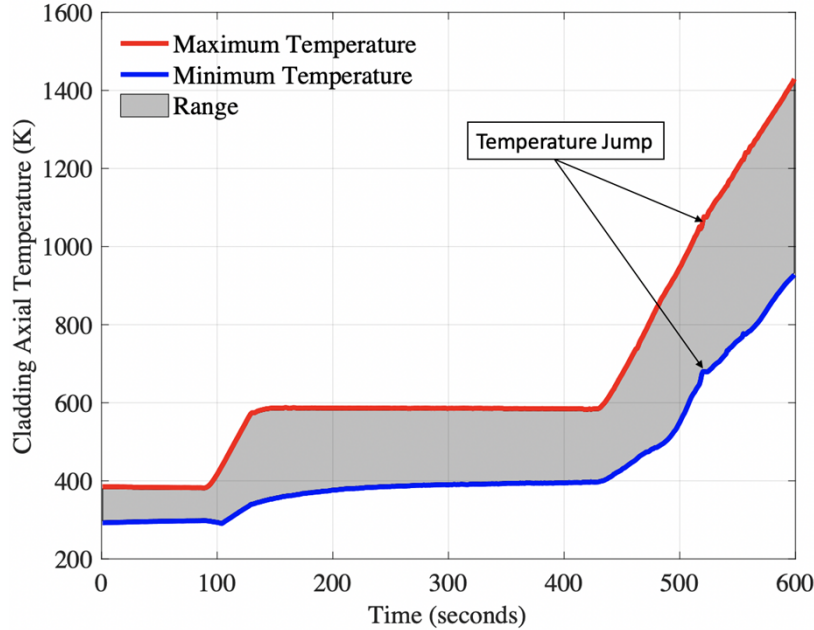


**Figure 7. Example of the temperature range from the fitted axial temperature profile.**

IR furnaces can cause azimuthally varying temperature profiles in similar burst testing facilities and were studied in greater detail in Erbacher et al. [16]. These temperature variations were experimentally measured and reported to reach up to 50°C. Therefore, for these tests, the two thermocouples attached 180° apart at the axial midplane of the cladding tube were used to identify variation and derive an azimuthal temperature factor.

This factor is calculated by dividing the temperature in the front of the cladding tube by the temperature in the back of the tube and was used to generate a cosine function that varies along the outer circumference of the cladding tube. The cosine function produces a nonuniform azimuthal temperature variation and is combined with the axial temperature profiles to generate a fully 3D time-dependent temperature surface for each test performed in the SATS. These temperature surfaces are used as boundary conditions input into BISON fuel performance simulations.

As shown by the azimuthal temperature factor in Figure 8, the back of the cladding tube is consistently hotter than the front. This difference between the two temperatures further diverges when the IR heater is active during heat-up phases. This can be observed when overlaying Figure 7 and Figure 8. Because the front of the cladding tube is continually cooler than the back, cladding tube ballooning is expected to be asymmetrical where the balloon strain is greater on the hotter side of the tube. Not accounting for the asymmetric behavior will result in inaccurate balloon strain prediction.

This manuscript has been authored by UT-Battelle, LLC under Contract No. DE-AC05-00OR22725 with the US Department of Energy (DOE). The US government retains and the publisher, by accepting the article for publication, acknowledges that the US government retains a nonexclusive, paid-up, irrevocable, worldwide license to publish or reproduce the published form of this manuscript, or allow others to do so, for US Government purposes. DOE will provide public access to these results of federally sponsored research in accordance with the DOE Public Access Plan (<http://energy.gov/downloads/doe-public-access-plan>).

<sup>2</sup> Corresponding author: [cappsna@ornl.gov](mailto:cappsna@ornl.gov)

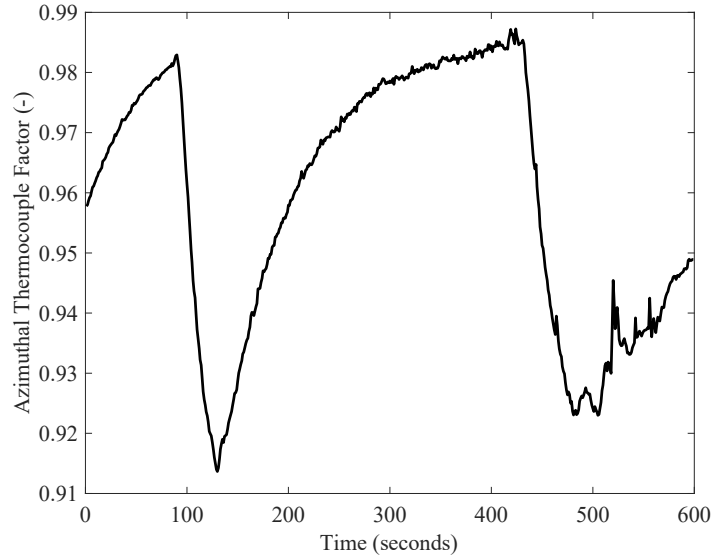


**Figure 8. Example of the azimuthal thermocouple factor that reports the relative difference in the temperature from the front and back of the cladding. A value of less than 1 indicates a temperature that is hotter on the cladding back side than the cladding front side.**

## 2.3 FINITE-ELEMENT MODEL

The BISON fuel performance code was used to simulate the cladding performance under the transient conditions. BISON is a nuclear fuel-specific, finite-element analysis code built on the MOOSE (Multiphysics, Object-Oriented Simulation Environment) Framework [9]. MOOSE employs a Jacobian-free Newton-Krylov method to solve coupled systems of nonlinear partial differential equations with parallel computing [10]. The expandability of the MOOSE framework gives BISON users the flexibility to incorporate empirical materials and behavioral or mechanistic models for integral fuel performance evaluations. This flexibility extends to material-specific constitutive properties, fuel rod or cladding tube geometry, and boundary conditions generated from the experimental data [11].

Evaluating the cladding performance under simulated LOCA conditions requires constitutive properties for the alumina rod (simulated fuel pellets), zirconium-based claddings, and chromium coating. Additionally, this finite element model used a discrete geometry for the chromium coating applied to the Zircaloy substrate. The alumina rod may provide a thermal sink comparable to  $UO_2$ , although it does not contribute any thermal energy or structural support to the system. Therefore, elastic and thermal material properties (i.e., thermal conductivity, specific heat, and thermal expansion) are the only models required for the alumina [12].

Similarly, Zry-4 cladding and chromium mechanical properties (i.e., elastic, thermal, and creep) are required to accurately simulate the cladding performance. The elastic modulus, Poisson's ratio, thermal expansion strain, thermal conductivity, and specific heat are all calculated for the zirconium-based alloys by using correlations from MATPRO [13]. The thermal creep model is divided into a composition-specific, low-temperature correlation, as in other works [14, 15], and a high-temperature creep phase-dependent model, as in Erbacher et al. [16]. The parameters used in the high-temperature creep model are based on the material phase ( $\alpha$ ,  $\alpha+\beta$ , and  $\beta$ ). A Zircaloy phase model change was implemented from a previous work and determined the phase of Zircaloy during LOCA transient [17]. Properties for the chromium coating include fitted correlations for temperature-dependent thermal conductivity, specific heat, and elastic modulus [18]. The thermal creep model used to simulate chromium is a Norton creep model fitted to data from previous thermal creep tests [18, 19]. The aforementioned models for the

zirconium-based claddings and the chromium coating were developed during previous studies and were distributed with BISON.

Thermal creep is the dominant deformation mechanism responsible for cladding ballooning and rupture. Zircaloy rupture during a LOCA is a result of plastic instability (i.e., loss of structural stability), and the cladding is assumed to fail when the creep rate reaches  $\sim 2.78\%/s$ . This value is consistent with previous work that modeled cladding plastic instability in fuel performance codes [20]. Previous work indicated that these rupture criteria provide an accurate comparison to the rupture temperature and time to burst; however, the cladding strain profile is greatly underpredicted [21]. For this analysis, the engineering stress—which was calculated with the internal pressure—and cladding temperatures were compared. Planned upgrades to this experimental equipment are expected to allow for in situ true strain comparisons between the cladding tube and simulation results. Lastly, there are no rupture criteria for chromium-coated cladding, and the coating thickness might affect the rupture behavior. In this analysis, the coating thickness (7  $\mu m$ ) was not expected to significantly affect the cladding rupture criteria; thus, a creep rate of  $2.78\%/s$  was deemed to be applicable to the tested cladding tubes.

The cladding tube geometries were generated using the parameters described in Table 1. The coating was modeled as a distinct domain applied to the cladding outer surface. This model did not include any transition layers associated with the coating application, nor did this model allow delamination or debonding of the coating. Future work and experimental testing are needed to better determine coating adherence and delamination. Each simulation is a fully 3D  $180^\circ$  cladding tube with the zero-displacement constraints on the bottom of the cladding tube. An axial slice of the cladding was made to prevent rigid body motion. These simulations used  $180^\circ$  symmetry, which fully incorporated the azimuthal and axial temperature variations while reducing the total computing resource usage required for a full-tube model.

The cladding end plugs were assumed sealed to easily calculate the gas internal volume. The internal gas volume comprises two separate volumes: (1) a volume calculated inside the tube itself, which heats and expands, increasing the internal pressure, and (2) a miscellaneous volume held at room temperature, which is used to represent the remaining gas held in other parts of the system. This gas sits in gas lines, fittings, valves, and a pressure transducer outside the cladding tube itself. Because this volume is unknown, the volume must be calibrated for this test based on pressure measurements during the initial temperature ramp to  $\sim 573$  K. Effectively, this model uses as a gas reservoir that dampens pressure changes within the cladding tube. The reservoir volume and temperature did not change, but the pressure remained in equilibrium with the cladding tube.

The only external boundary conditions applied to this model were the 3D temperature profiles, as described previously, and the initial pressure. These temperatures were applied to the cladding surface as Dirichlet boundary conditions at each time step. Because the simulations assess the volume, temperature, and pressure of the internal gas together from room temperature, the internal pressure was set to closely match the pressure of the burst experiments during the first holding period after the pressure regulator was set, the gas valves were closed, and the tube was sealed. These simulations were operated through the first holding period until the heating phase and were terminated when the cladding creep strain rate threshold was reached.

This manuscript has been authored by UT-Battelle, LLC under Contract No. DE-AC05-00OR22725 with the US Department of Energy (DOE). The US government retains and the publisher, by accepting the article for publication, acknowledges that the US government retains a nonexclusive, paid-up, irrevocable, worldwide license to publish or reproduce the published form of this manuscript, or allow others to do so, for US Government purposes. DOE will provide public access to these results of federally sponsored research in accordance with the DOE Public Access Plan (<http://energy.gov/downloads/doe-public-access-plan>).

<sup>2</sup> Corresponding author: [cappsna@ornl.gov](mailto:cappsna@ornl.gov)

### 3. RESULTS

#### 3.1 COMPARISON WITH SATS DATA

3D temperature boundary conditions were generated from individual cladding burst tests of coated and uncoated zirconium-based alloys and implemented into BISON. An illustration of the resulting temperature surface generated during a simulation is shown in Figure 9. The figure highlights the 3D temperature surface at the time of burst for the uncoated 800 psi Zr-4 burst test. This example shows a hot spot generated in the cladding along the front near the lower span of the cladding tube. This local increase in the cladding tube temperature resulted in a localized increase in the creep strain rate and subsequent cladding failure.

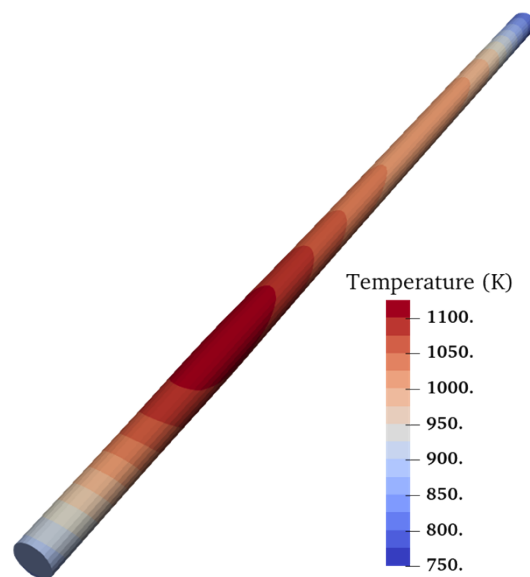


**Figure 9. 3D cladding surface temperature at the rupture temperature for the uncoated 800 psi Zr-4 burst test; geometry is reflected into a 360° model across the axial plane to better illustrate the temperature variation.**

The cladding tube pressure evolution during this same simulation is shown in Figure 10. In this simulation, the initial pressure was 5.75 MPa (shown in blue), whereas the data began at ~5.6 MPa (shown in red). Because of the different starting pressures, the pressure throughout the holding phase was slightly different; however, the pressure in the experiment slowly increased to reach a similar value before the heating phase. This was assumed to occur because the gas volume was heated external to the cladding tube. As the heat-up phase began, the pressures in both the simulation and the experiment increased similarly. Because the simulation was terminated before extensive deformation could occur, the pressure data did not show the same shoulder observed in the experiment data. The shoulder is observed in the experimental data and evident when the pressure starts decreasing from the peak pressure. This was an effect from the high-temperature cladding creep model and the failure criteria. Although the cladding deformation evolution was expected to be somewhat different, the time to failure and the temperatures were very similar, indicating that the boundary conditions provided accurate agreement between the model and experimental data.

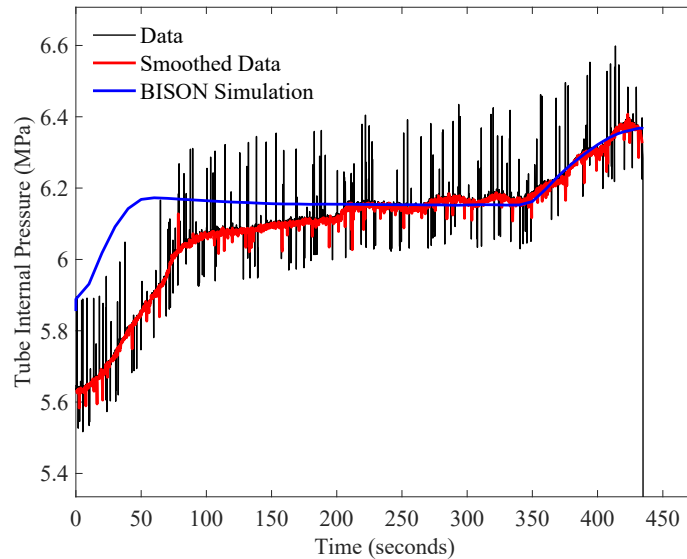


**Figure 10. Comparison of the pressure evolution between the data (black), a smoothed data representation (red), and simulation (blue) for the uncoated 800 psi Zr-4 burst test.**

This process was performed for eight Zry-4 tubes: four coated and four uncoated. The rupture temperature and cladding hoop stress are shown in Figure 11. Figure 11a compares the simulation results with the measured thermocouple locations (i.e., historical approach) in which the rupture temperature from the simulations was sampled only at the locations on which thermocouples would be attached. Figure 11b shows the experimental data against simulations in which the peak cladding temperature at any point along the cladding surface was reported. The two figures delineate the cladding burst temperature and hoop stress based on simulation or data (reds vs. blues) and uncoated or coated tubes (red and blue vs. magenta and cyan). The burst criterion from Chapman et al. [22] is shown here for illustrative purposes and was calculated for a heating rate of  $6^{\circ}\text{C/s}$ . This heating rate was calculated from the average cladding surface heating rate measured during the experiment, although the reported control thermocouple in the SATS shows  $5^{\circ}\text{C/s}$ .

This manuscript has been authored by UT-Battelle, LLC under Contract No. DE-AC05-00OR22725 with the US Department of Energy (DOE). The US government retains and the publisher, by accepting the article for publication, acknowledges that the US government retains a nonexclusive, paid-up, irrevocable, worldwide license to publish or reproduce the published form of this manuscript, or allow others to do so, for US Government purposes. DOE will provide public access to these results of federally sponsored research in accordance with the DOE Public Access Plan (<http://energy.gov/downloads/doe-public-access-plan>).

<sup>2</sup> Corresponding author: [cappsna@ornl.gov](mailto:cappsna@ornl.gov)

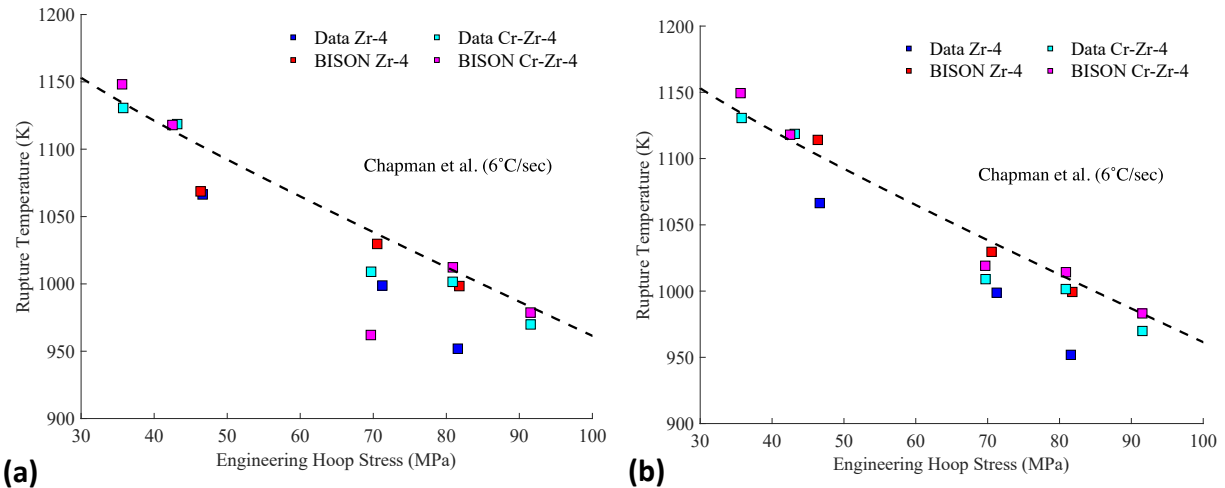


**Figure 11. Cladding rupture temperature vs. engineering hoop stress for all burst tests and corresponding simulations. (a) BISON data (red and magenta) use the peak thermocouple temperature to make a consistent comparison with the experimental data, whereas (b) BISON data use the peak temperature on the cladding surface.**

The BISON results in Figure 11a generally predicted higher cladding rupture temperatures than the experimental data. However, by considering the peak temperature at any point on the cladding surface, as shown in Figure 11b, results in a better comparison between the simulation results and experimental data. These results highlight the need for new methods for characterizing cladding temperatures in situ to ensure that the temperature at the burst location is accurately determined. The chromium-coated cladding burst tests were expected to show some amount of added cladding structural stability; however, the effect of the coating on these simulations was barely discernable because of the coating thickness. These results indicate that the coating does not negatively affect the cladding behavioral response. This model does not include degradation mechanisms of the coating, such as cracking, delamination, or spalling, which may further diminish the effect of the coating. Given the favorable comparison of the simulations and experiment, a short parametric evaluation was performed to identify the effect of the coating on the cladding at various initial pressures.

### 3.2 PARAMETRIC EVALUATION OF CLADDING BURST IMPACT FROM CHROMIUM COATING

A short parametric evaluation was performed to determine the effect of the chromium coating on the predicted cladding burst behavior. This set of simulations considered an uncoated and a 7  $\mu\text{m}$  chromium-coated Zry-4 cladding tube under the same operating conditions in which only the initial pressure was varied. The temperature boundary conditions for these simulations are from the 800 psi uncoated Zry-4 burst experiment. Figure 12 shows the results of this analysis in which the initial pressure varied from 3 to 14 MPa in 1 MPa increments. In this figure, the rupture temperature is the peak cladding temperature, and the lower error bars represent the peak thermocouple temperature. The results of this analysis demonstrate that the 7  $\mu\text{m}$  thick chromium coating can provide an approximately 10 K increase in the burst temperature. Although not significant, it highlights the potential for an increased burst temperature margin from thicker coatings. The analysis indicates a slight deviation in comparison to the Chapman rupture model around ~60-70 MPa. There are many possibilities for this deviation, however, most likely reason is related to the creep model being tuned to this specific burst regime. The existing coatings were poor in quality and improving the coating application process will likely have a significant impact. Additionally, the proposed coating thicknesses are expected to range up to three times what was evaluated in this work [23], and the current BISON results could suggest a coating thickness dependence on burst temperatures. Future burst testing and simulation results should better refine this margin. Additional work

is needed to determine the effect of intermediate phases that may form between the coating and the cladding. These results also show an increase of  $\sim 25\text{--}50\text{ K}$  by using the peak temperature instead of the peak thermocouple temperature for the burst criteria. This highlights the need to improved temperature characterization techniques in order to reduce rupture temperature uncertainties and increase simulation fidelity.

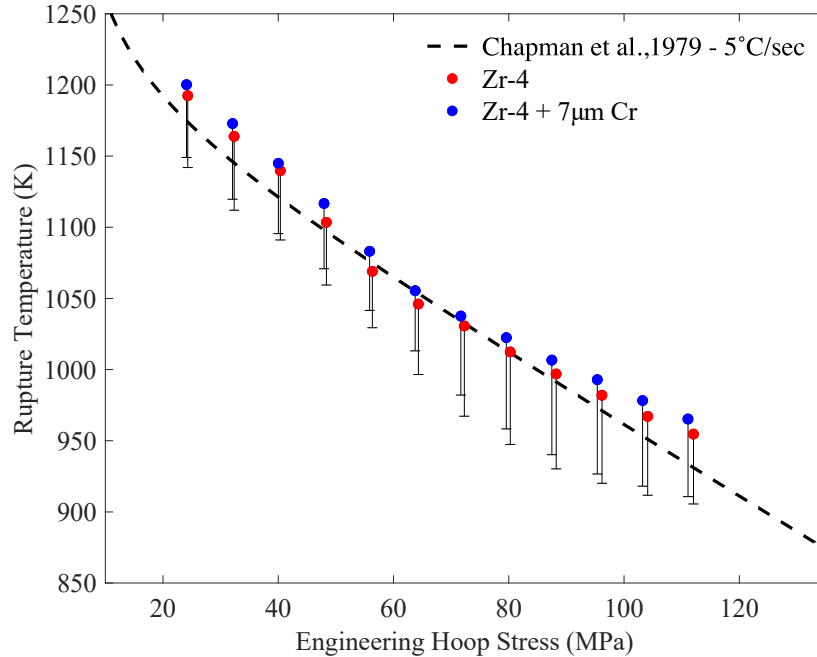


**Figure 12. Coated (blue) cladding simulations show an increased rupture temperature relative to uncoated (red) cladding. Marker temperatures show the maximum cladding temperature, and error bars show the peak thermocouple temperature.**

#### 4. CONCLUSIONS AND FUTURE WORK

This work demonstrated BISON’s ability to appropriately model coated cladding tubes using a multilayered approach as well as identify potential increases of the cladding margin to burst from the addition of the coating. The approach first developed a method to assess the full cladding tube surface temperature distribution, as a boundary condition for BISON cladding burst simulations. The initial investigation of coated claddings showed BISON capable of the analysis and the comparisons experimental data showed a potential increase in the cladding tube failure margin from the addition of the  $7\ \mu\text{m}$  chromium coating. Although the temperatures at failure and the pressure evolution showed relatively good agreement in this work, this is the first step of a larger effort to simulate the cladding deformation process and assess the cladding margin to failure more accurately. This example also demonstrates how fuel performance codes such as BISON can be used to model experiments and identify where greater attention is needed. By combining advanced modeling techniques with experimental data, simulations can be conducted to more accurately assess whether the burst experiments are capturing all the cladding behavior. This is most notably shown in the need to improve coating processes as well as the need to develop a composite high temperature creep model for chromium coated Zircaloy, and therefore,

This manuscript has been authored by UT-Battelle, LLC under Contract No. DE-AC05-00OR22725 with the US Department of Energy (DOE). The US government retains and the publisher, by accepting the article for publication, acknowledges that the US government retains a nonexclusive, paid-up, irrevocable, worldwide license to publish or reproduce the published form of this manuscript, or allow others to do so, for US Government purposes. DOE will provide public access to these results of federally sponsored research in accordance with the DOE Public Access Plan (<http://energy.gov/downloads/doe-public-access-plan>).

<sup>2</sup> Corresponding author: [cappsna@ornl.gov](mailto:cappsna@ornl.gov)

future work will include a comparison of in-situ cladding strain profiles between the simulation and experiment. This will contribute to the development and eventual implementation of a new cladding creep model specifically for chromium coated Zircaloy tubes. Additionally, identifying any coating effects that arise during steady-state operation is also planned. This includes implementing coating irradiation properties and a power-law strain-hardening plasticity model. These models will then be applied to a full-length rod analysis to compare steady-state performance impacts from coated cladding.

## 5. REFERENCES

1. Cathcart, J., et al., *Zirconium metal-water oxidation kinetics. IV. Reaction rate studies*. 1977, Oak Ridge National Lab.
2. Moalem, M. and D.R. Olander, *Oxidation of Zircaloy by steam*. Journal of Nuclear Materials, 1991. **182**: p. 170-194.
3. Hofmann, P., *Current knowledge of core degradation phenomena, a review*. Journal of Nuclear Materials, 1998. **270**: p. 194-211.
4. Terrani, K., *Accident tolerant fuel cladding development: Promise, status, and challenges*. Journal of Nuclear Materials, 2018.
5. Brachet, J.-C., et al., *Early studies on Cr-Coated Zircaloy-4 as enhanced accident tolerant nuclear fuel claddings for light water reactors*. Journal of Nuclear Materials, 2019. **517**: p. 268-285.
6. Geelhood, K. and W. Luscher, *Degradation and Failure Phenomena of Accident Tolerant Fuel Concepts: Chromium Coated Zirconium Alloy Cladding*. 2019, Pacific Northwest National Laboratory: Richland, Washington.
7. Snead, M.A., et al., *Severe Accident Test Station Design Document*. 2015, ; Oak Ridge National Lab. (ORNL), Oak Ridge, TN (United States). p. Medium: ED; Size: 62 p.
8. Massey, C.P., et al., *Cladding burst behavior of Fe-based alloys under LOCA*. Journal of Nuclear Materials, 2016. **470**: p. 128-138.
9. Williamson, R.L., et al., *Multidimensional multiphysics simulation of nuclear fuel behavior*. Journal of Nuclear Materials, 2012. **423**(1-3): p. 149-163.
10. Gaston, D., et al., *MOOSE: A parallel computational framework for coupled systems of nonlinear equations*. Nuclear Engineering and Design, 2009. **239**(10): p. 1768-1778.
11. Hales, J., et al., *BISON Theory Manual The Equations Behind Nuclear Fuel Analysis*. 2016, Idaho National Laboratory (INL), Idaho Falls, ID (United States).
12. Auerkari, P., *Mechanical and physical properties of engineering alumina ceramics*. Vol. 23. 1996: Technical Research Centre of Finland Espoo.
13. Hagrman, D.T., C.M. Allison, and G.A. Berna, *SCDAP/RELAP5/MOD 3.1 code manual: MATPRO, A library of materials properties for Light-Water-Reactor accident analysis. Volume 4*. 1995.
14. Limbäck, M. and T. Andersson. *A model for analysis of the effect of final annealing on the in-and out-of-reactor creep behavior of zircaloy cladding*. in *Zirconium in the Nuclear Industry: Eleventh International Symposium*. 1996. ASTM International.
15. Matsuo, Y., *Thermal Creep of Zircaloy-4 Cladding under Internal Pressure*. Journal of Nuclear Science and Technology, 1987. **24**(2): p. 111-119.

16. Erbacher, F., et al., *Burst Criterion of Zircaloy Fuel Claddings in a Loss-of-Coolant Accident*, in *Burst Criterion of Zircaloy Fuel Claddings in a Loss-of-Coolant Accident*. 1982.
17. Pastore, G., et al. *Modeling of fuel behavior during loss-of-coolant accidents using the BISON code*. in *2015 LWR Fuel Performance Meeting—Top Fuel, Zurich, Switzerland*. 2015.
18. Wagih, M., et al., *Fuel performance of chromium-coated zirconium alloy and silicon carbide accident tolerant fuel claddings*. *Annals of Nuclear Energy*, 2018. **120**: p. 304-318.
19. Stephens, J.R. and W.D. Klopp, *High-temperature creep of polycrystalline chromium*. *Journal of the Less Common Metals*, 1972. **27**(1): p. 87-94.
20. Di Marcello, V., et al., *The TRANSURANUS mechanical model for large strain analysis*. *Nuclear Engineering and Design*, 2014. **276**: p. 19-29.
21. Capps, N.A. and R.T. Sweet, *Characterization of Modeling and Experimental Data Inconsistencies from Burst Testing for High-Burnup Commercial Fuel Rod Applications*. *Manuscript in Review*, 2021.
22. Chapman, R.H., et al., *Zirconium Cladding Deformation in a Steam Environment with Transient Heating*, J.H. Schemel and T.P. Papazoglou, Editors. 1979, ASTM International: West Conshohocken, PA. p. 393-408.
23. Geelhood, K. G., and W. G. Luscher. "Degradation and Failure Phenomena of Accident Tolerant Fuel Concepts: Chromium Coated Zirconium Alloy Cladding." *Pacific Northwest National Laboratory* 96 (2019).

This manuscript has been authored by UT-Battelle, LLC under Contract No. DE-AC05-00OR22725 with the US Department of Energy (DOE). The US government retains and the publisher, by accepting the article for publication, acknowledges that the US government retains a nonexclusive, paid-up, irrevocable, worldwide license to publish or reproduce the published form of this manuscript, or allow others to do so, for US Government purposes. DOE will provide public access to these results of federally sponsored research in accordance with the DOE Public Access Plan (<http://energy.gov/downloads/doe-public-access-plan>).

<sup>2</sup> Corresponding author: [cappsna@ornl.gov](mailto:cappsna@ornl.gov)